CLM-P701

CLM-P701

UKAEA

Preprint

THE STRUCTURE OF MAGNETIC FLUCTUATIONS IN HBTX1A REVERSED FIELD PINCH

I. H. HUTCHINSON
M. MALACARNE
P. NOONAN
D. BROTHERTON-RATCLIFFE

CULHAM LABORATORY
Abingdon Oxfordshire

1983

CLM-P 701

THE STRUCTURE OF MAGNETIC FLUCTUATIONS IN HBTX1A REVERSED FIELD PINCH

I H Hutchinson*, M Malacarne+, P Noonan and D Brotherton-Ratcliffe≠

Culham Laboratory, Abingdon, Oxfordshire, OX14 3DB, UK

(Euratom/UKAEA Fusion Association)

ABSTRACT

Arrays of edge magnetic coils and statistical analysis techniques have been used to investigate the magnetic fluctuation structure in HBTX1A Reversed Field Pinch. The superficially random fluctuations can in fact be attributed almost entirely to global modes with poloidal mode number m = 0 and 1 provided account is taken of toroidal distortion of the modes. A toroidal array of coils discloses a broad spectrum of toroidal mode numbers with peak at $|n| \sim 10$ and significant variation with time and frequency. Cross correlation establishes that the $|n| \sim 10$ is m = 1, a helical mode resonant inside the reversal surface and also shows the presence of m = 0, $n \sim 0$. The timescales of the fluctuation indicate that the instabilities are probably resistive in character and mode amplitudes are such that island overlap and magnetic field ergodization should occur. The energy confinement time due to stochastic transport, estimated from the measured fluctuations, is consistent with that experimentally observed.

* Present Address: Nuclear Engineering Department, Massachusetts Institute of Technology, Cambridge, Ma 02139, USA.

+ Euratom supported Fellow and Oxford University, UK.

≠ Royal Holloway College, London University, UK.

(Submitted for publication in Nuclear Fusion)

July 1983

1. INTRODUCTION

In the Reversed Field Pinch (RFP), even during relatively quiescent periods, there exists a significant level of fluctuation in the magnetic field. It is widely accepted that the appearance and sustainment of reversed magnetic field by plasma action requires such magnetic fluctuations, although the detailed mechanisms by which self reversal occurs are generally not yet understood. It also seems that usually the energy confinement in the RFP is determined by enhanced transport arising from the fluctuations. Detailed study of the fluctuations therefore offers the possibility of elucidating these two vital topics: self reversal mechanisms and energy transport. We present here a study of magnetic fluctuation in the RFP HBTX1A using magnetic coils outside the plasma edge.

Magnetic fluctuations have long been observed in stabilised pinch discharges, and in early experiments on ZETA and Mk IV torus [1, 2] clear evidence of principally kink (m = 1) modes was obtained. Later ZETA experiments [3] concentrated on higher frequencies and upon interpretation in terms of fully developed turbulence and less attention was paid to the larger scale lengths. In fast programmed experiments on HBTX [4] coherent m = 1 kinks were also observed during sustainment; these perturbations appeared to be a mixture of ideal and resistive modes.

More recently on present generation pinches, studies have been reported on ETA-BETA II [5] and OHTE [6]. In the latter case, results very similar to the early ZETA and Mk IV torus results were obtained, indicating dominantly m = 1 modes.

The experimental techniques for studying magnetic fluctuations using magnetic coils of various sorts are of course well developed. In addition to magnetic probes inserted into the plasma, which have been used both in RFPs [6] and Tokamaks [7], coils outside the plasma in the form of discrete coils or coils specially wound to measure Fourier components (sine and cosine coils) have proven of considerable help in diagnosing plasma instabilities and are now used routinely in Tokamaks.

Two important factors distinguish our techniques from those which are most frequently used. The first is that in the RFP the most dangerous MHD instabilities [8, 9] have poloidal mode number m = 0 or 1 and a variety of possible toroidal mode numbers, n. This is the converse of the Tokamak situation with dominantly n = 1 (or 2) and various m, and implies that it is of considerable interest to have arrays of coils round the toroidal circumference rather than just the poloidal circumference as is more usual. The second factor is that the majority of RFP fluctuations do not have the obvious periodicities in time which are typically seen in Tokamaks; rather, the fluctuations appear to be fairly stochastic and turbulent. The consequence of this is that in many cases it is not possible to distinguish the evolution of particular types of modes simply by inspection. It is therefore usually necessary to adopt statistical forms of analysis in order to extract from the apparently random signals the required information.

Our studies here concentrate on the sustainment phase of the RFP discharge during which the fluctuations are weakest and also typically least coherent. We present systematic analysis of the poloidal and toroidal mode structure and of helical perturbations. In addition we present observations of the evolution of the perturbations, very low frequency oscillations and

some observations of the termination phase. In the final section we discuss the interpretation of our results in terms of the resistive MHD instabilities expected in RFP configurations.

2. TECHNIQUES

Details of the HBTX1A experiment have been published elsewhere [10]. The magnetic coils used in these studies consist primarily of three sets illustrated in Fig 1. Outside the vacuum liner, in the interspace between the liner (inner minor radius 0.26 m, major radius R = 0.8 m) and the conducting shell (inner minor radius 0.29 m) we have a poloidal array of coils measuring toroidal and poloidal components of the field (B_ϕ, B_θ) at 16 poloidal angles (θ). Also, adjacent to the poloidal array, is a toroidal array measuring B_ϕ and B_θ at 14 toroidal positions covering 60° in toroidal angle. The toroidal array is at a poloidal angle of -40°. Inside the vacuum vessel are poloidal arrays similar to the interspace array but with the coils recessed into special sections of the bellows liner. These internal coils are more sensitive to higher frequency fluctuations because they do not require the fields to penetrate the liner.

The signals from these coils, either integrated or unintegrated, are digitised typically at 500 kHz sampling frequency using 10 bit ADCs (LeCroy 8210). Because of the nature of the signals this is fast enough to avoid aliasing problems (except possibly at high frequencies with the unintegrated internal coils) and to cover the frequency band in which virtually all the fluctuation power lies.

A variety of forms of statistical analysis has been applied to the signals obtained which we summarise here. Given signals x(t), y(t) during a finite time period T with Fourier transforms $X(\nu)$, $Y(\nu)$, which we calculate numerically by FFT programs, the power spectrum of x is

$$P_x(\nu) \equiv \frac{1}{T} \langle |X(\nu)|^2 \rangle$$

where <> denotes average over ensembles (i.e. distinct time periods or different shots). The cross spectrum is given by

$$\Gamma(\nu) = \frac{1}{T} \langle X(\nu)\, Y^*(\nu) \rangle$$

and $|\Gamma|$ is commonly called the cross power spectrum and $\arg(\Gamma)$ the phase spectrum; these are useful for discovering any systematic phase relationships between the signals x and y. The normalised cross spectrum

$$\gamma = |\Gamma| / [P_x P_y]^{1/2}$$

is called the coherence.

In the time domain we use the cross correlation function

$$R_{xy}(\tau) \equiv \left\langle \frac{1}{T} \int x(t)\, y(t+\tau)\, dt \right\rangle$$

which we often normalise to give the cross correlation coefficient:

$$\rho(\tau) = R_{xy}(\tau) / [R_{xx}(0)\, R_{yy}(0)]^{1/2}$$

We note that for signals which are statistically stationary the Wiener-Kintchine theorem states that $P_x(\nu)$ is the Fourier transform of R_{xx}.

It is often convenient to perform time domain correlation analysis for signals which are frequency filtered in various ways. For example this may be used to remove the slow variations due to equilibrium evolution. In order to do this we multiply the Fourier spectrum $X(\nu)$ by an appropriate filtering function (e.g. a 'box' $f(x) = 1$ for $\nu_1 < \nu < \nu_2$, zero elsewhere) and then transform back to obtain the filtered time history $x'(t)$ which can then be used to obtain correlations. In this way we can concentrate on fluctuations in a limited frequency range, excluding others.

The structure of the fluctuations in the spatial coordinates θ and ϕ is often most easily expressed as an expansion in terms of spatial Fourier harmonics: $\exp i(m\theta + n\phi)$. We can form linear combinations of the discrete coil signals in order to obtain the time histories of various poloidal or toroidal harmonics. These can then be used as input to the various statistical coefficients outlined above. An alternative approach is to investigate the cross correlation of the magnetic fluctuations at various positions e.g. forming the autocorrelation in space. In essence this approach contains the same information as the spatial harmonics; however it sometimes provides a more transparent interpretation and sometimes allows greater resolution.

3. RESULTS

3.1 General

The evolution of the main discharge parameters for a typical shot of interest is shown in Fig 2. We will present mostly data for shots such as this whose plasma current is sustained approximately constant at ~ 200 kA. Brief surveys of other discharges show little substantial change in the character of the fluctuations in shots with decaying curretns. Substantial surveys over different current level, pinch parameter or filling pressure have not yet been carried out.

Also shown in Fig 2 are example traces from single coil probes: integrated giving field B_ϕ and unintegrated giving $\dot{B}_\theta$. The apparently stochastic nature of the fluctuations is evident from these traces.

The power spectrum, $P(\nu)$, during the current sustainment phase of such signals is shown in Fig 3. These spectra are averaged over 5 shots to illustrate the trends, though substantial variation from shot to shot occurs in the details of the spectra. It is clear that the dominant power is at low frequencies. Above about 40 kHz the spectra fall off approximately as ν^{-2}. As can be observed in the figure there is little obvious difference in the spectral shape for B_θ and B_ϕ although the power at the lower frequencies ($\lesssim$ 40 kHz) is systematically slightly higher for B_ϕ.

The total rms fluctuation levels expressed as a fraction of the (poloidally averaged) total magnetic field, $(B_\phi^2 + B_\theta^2)^{1/2}$, are plotted in Fig 4 as a function of poloidal angle θ. The significant variation particularly in $\tilde{B}_\theta$ is indicative of the importance of toroidicity in HBTX1A. The mean fluctuation levels are typically 1.5% for B_ϕ and 1% for B_θ during sustainment and considerably greater, 6 - 10% for both, during current rise and termination.

3.2 Poloidal Mode Structure

In order to determine the structure of the fluctuations we may Fourier decompose in θ by forming the sums over coils k:

$$C_m = \frac{2}{N} \sum_{k=1}^{N} \tilde{B}_k . \cos m\theta_k$$

$$S_m = \frac{2}{N} \sum_{k=1}^{N} \tilde{B}_k . \sin m\theta_k$$

and

$$P_m = \tfrac{1}{2} < \left|C_m\right|^2 + \left|S_m\right|^2 >$$

which then gives the total power in each Fourier mode. In Fig 5 we plot the resultant poloidal mode power spectra obtained from the internal coil array during the sustainment phase. The spectrum of $\tilde{B}_\phi$ is dominated by m = 0, 1 with very rapid fall off at higher m; while for $\tilde{B}_\theta$ the spectrum, though similar, shows relatively rather greater levels of m = 2 and less m = 0.

Another approach to the poloidal mode structure is to form the cross correlation coefficient (initially with zero time delay) between the various coils thus giving the spatial autocorrelation. This is shown for B_θ in Fig 6 using coils approximately on the inner(a) and outer(b) equator as

reference coil. There is a very clear difference in the autocorrelation obtained with these different references; using references at $\theta \simeq \pm 90°$ gives autocorrelations which are asymmetric. These differences indicate that the fluctuations do not possess rotational symmetry in their statistics: i.e. θ is not an ignorable coordinate. The nature of the fluctuations may be deduced from inspection of such autocorrelations. To lowest order, disregarding for a moment the lack of rotational symmetry, the autocorrelation is that which would be expected from dominantly m = 0 and m = 1 of similar magnitude i.e. it is the sum of a constant plus a $\cos\theta$ dependent part. The lack of symmetry indicates that in fact the "m = 1" component is distorted due to toroidicity so that its phase varies more rapidly at the outer equator ($\theta \sim 0$) than the inner ($\theta \sim 180°$).

Expressed in terms of the Fourier decomposition, this means that the fluctuation mode consists of a sum of poloidal Fourier components,

$$M_1 = \cos(\theta - \alpha) + \varepsilon_2 \cos(2\theta - \alpha) + \ldots$$

where α is some (random) phase, these Fourier components being coupled (linearly) together. The signature of this linear coupling is that the $\cos\theta$ and $\cos 2\theta$ (and also $\sin\theta$ and $\sin 2\theta$) components are always in phase with each other. This characteristic is readily confirmed by forming the cross-spectrum between $\cos\theta$ and $\cos 2\theta$. Fig 7 shows this spectrum. The coherence at lower frequencies is very high ($\gtrsim 0.8$) indicating that about 60% of the power in the modes is linearly coupled. The phase is zero indicating that the $\cos 2\theta$ and $\cos\theta$ are in phase at $\theta = 0$ (the outer equator) as expected from the autocorrelation data. The fall off of coherence and accompanying randomisation of the phase at higher frequencies for this spectrum appears

to be caused by the increasing importance of electronic system noise owing to the fall in power. Coherence spectra obtained by using unintegrated $\dot{B}$ signals do not suffer from this problem and coherence is high right out to 250 kHz. It is possible also that different modes become important at higher frequency.

The spatial autocorrelation of $\tilde{B}_\phi$ shows less asymmetry than $\tilde{B}_\theta$ although the m = 1 m = 2 coherence spectrum is qualitatively similar, indicating that there is some linear coupling. This is consistent with the mode spectra showing smaller m = 2 power for $\tilde{B}_\phi$ than $\tilde{B}_\theta$.

Fig 8 illustrates a different type of linear coupling observed in the m = 0 m = 1 cross spectrum of B_ϕ. In this case at the higher frequencies the cross phase is 180° indicating that the modes add constructively at the inner equator. This is consistent with the toroidal distortion of the m = 0 mode which is that $B_\phi \propto 1/R \simeq 1 - (a/R_0)\cos\theta$. The lower coherence at low frequencies indicates that the major parts of the m = 0 and m = 1 power there are independent.

The poloidal mode structure is thus that there are dominantly just two statistically significant types of mode M_0 and M_1 which may be identified as the modes corresponding to m = 0 and m = 1 plus their concomitant higher harmonics generated by the toroidal distortions. These linear coupling effects are stronger for $\tilde{B}_\theta$ than $\tilde{B}_\phi$ which is partly why the mode spectra are different. The presence of higher order modes independent of M_0, M_1 is not established; however their power is certainly less than 3% of the M_0 and M_1 power.

In order to determine propagation and rotation effects we examine the time delayed cross correlation between coils in the poloidal array. Fig 9(a) shows the result for $\tilde{B}_\theta$ in which evidence of rotation is indeed present. The direction of rotation is in the ion diamagnetic drift direction (which is in the direction of electron poloidal current flow) inside the reversal surface. The rapid fall off with time (or distance) of the maximum value of the time delayed correlation coefficient indicates the relative incoherence of the modes due either to a broad spread of rotation rates or to growth and decay rates of the same order of magnitude as the rotation.

That there are different rotation rates is emphatically confirmed by Fig 9(b) in which the time delayed cross correlation for $\tilde{B}_\phi$ shows rotation for nominally identical shots in the opposite direction to $\tilde{B}_\theta$ rotation. This is not due to shot to shot variation since it is observed on a single shot, but must presumably be interpreted as an indication that in this case the fluctuations to which $\tilde{B}_\phi$ is most sensitive preferentially rotate in the opposite direction to those to which $\tilde{B}_\theta$ is most sensitive. Other sets of discharges of nominally similar parameters sometimes show almost no significant rotation. The reasons for this are unclear.

3.3 Toroidal Mode Structure

We have used the toroidal array of coils to determine the toroidal mode structure of the fluctuations initially by forming cross-correlations within the toroidal array to give the toroidal autocorrelation in space. If the machine were completely toroidally symmetric then ϕ would be an ignorable

coordinate and the cross correlation between two angles ϕ_1 and ϕ_2 would depend only on $|\phi_1 - \phi_2|$. In Fig 10 we show the spatial autocorrelation averaged over the sustainment phase obtained for $\phi > 0$ by using coil 1 of the toroidal array as reference and for $\phi < 0$ using coil 14 as reference. The symmetry obtained is not perfect, indicating that the fluctuations' properties are not perfectly toroidally symmetric, presumably due to the presence of ports, shell gaps, etc which introduce asymmetries into the machine.

The spatial autocorrelation has a rapidly damped form indicating a fairly broad spectrum of toroidal wavelengths. It is clear that a close spaced array of the type we are using is essential for obtaining a reasonable estimate of the toroidal structure since the correlation length is of the order of or less than the 60° in ϕ which we have available. Thus it would not be possible to obtain detailed information on the toroidal structure except with arrays whose spacing is considerably less than this 60° correlation length. It would be preferable to have a toroidal array whose extent was much greater than the correlation length. Unfortunately the present array does not meet this criterion and the result is that our resolution of toroidal wave number is of the same order as the width of its spectrum. This enforces upon us the need to maximise the resolution in our data analysis.

In order to obtain the toroidal wave number spectrum, which we express in terms of the mode number $n(\equiv 2\pi R k_\phi)$, we symmetrize the autocorrelation function by averaging the two sides of Fig 10 and then Fourier transform. This is equivalent to taking the cosine transform only of the unsymmetrized autocorrelation and discarding the sine transform. This process provides

nearly twice the resolution obtainable by forming directly weighted sums of coil signals but requires us to invoke the approximate ignorability of ϕ. The results we obtain are consistent with the direct method.

Resulting n-spectra are shown for B_ϕ in Fig 11. The inset shows the shape function we obtain by this process, the spectra obtained being the convolution of this shape function with the true spectra. We show results for several frequency bands obtained by digital filtering. It may be observed that the detailed shape of the spectrum changes with frequency. The dominant feature at most lower frequencies is at n = 8 - 12 and there sometimes appears to be higher harmonic structure to the spectrum. Generally very little power appears for $n \lesssim 5$, although some other spectra show power close to n = 0.

Propagation in the toroidal direction has been observed from time delayed cross correlation coefficients. Fig 12 shows a typical example. The propagation is generally even less pronounced than that observed on the poloidal array in Fig 7 indicating the incoherence of the modes. At the lower frequencies where the rotation is generally least ambiguous the observed direction of preferred rotation is in the direction of (conventional) toroidal plasma current (i.e. opposite to the electron flow). The speed is essentially given by the frequency and preferred n and is typically 10^4 ms^{-1}.

3.4 Helical Mode Analysis

Although the results presented so far give a general picture of the m and n spectra separately they do not of themselves allow us to determine the

mode structure and associate given m's with certain n's. This requires in general a two dimensional array of measurements which can then be decomposed into helical Fourier components of the form exp $i(m\theta + n\phi)$. Our situation is less complete than this in that we have only two perpendicular one-dimensional arrays.

If we form the 'correlation matrix',

$$Q(\theta,\phi) \equiv \langle x(\theta,\phi_o)\, x^*(\theta_o,\phi)\rangle$$

by correlating at zero time delay the signals from the poloidal array with those of the toroidal array we obtain a two dimensional measure of the statistical properties. In a situation in which θ and ϕ are ignorable it may be shown that Q is sufficient to determine essentially completely the second order statistics (i.e. power spectra, etc). In particular the Fourier transform of Q,

$$A_{mn} = \frac{1}{(2\pi)^2} \iint \exp\left[-i(m\theta + n\phi)\right]\, Q(\theta,\phi)\, d\theta\, d\phi$$

is then equal to the two dimensional power spectrum.

As we have shown above, toroidal effects are quite strong so that θ is not ignorable and some asymmetries exist even in the ϕ direction. Nevertheless we can form Q and transform it to obtain A which we refer to as the 'association spectrum' since it is a measure of the correlation between m and n components. We expect the linear coupling toroidal effects to

generate 'spurious' associations on A in adjacent m numbers but allowance can be made for this in interpreting the spectra produced.

Fig 13 shows an example of a correlation matrix for $\tilde{B}_\theta$ obtained from the two interspace arrays. Its maximum is near $\theta = -40°$ $\phi = 60°$ at the intersection of the arrays, and it clearly shows a dominantly diagonal correlation profile indicating a helical structure.

Transforming Fig 13 we get the corresponding association spectrum shown in Fig 14. The symmetry $A_{m\ n} = A^*_{-m-n}$ allows us to adopt the convention that m is taken always non negative and then n ranges from $-\infty$ to $+\infty$. Our sign convention is that magnetic field lines inside the reversal surface have helicity corresponding to negative n. Because the power is negligibly small for higher m we show only $m \leq 3$; also we plot only the real part of the transform since in the ideal case where θ,ϕ are ignorable and the ϕ range measured is $0 - 2\pi$ (neither of which is the case here) the imaginary part is zero. The inset shows the line width (convolution) function.

The dominant feature peaks at m = 1 n ≃ -7 with evidence of a tail extending out to n ~ -20. Additional peaks appear near n = 0 and n = +9 on m = 1 and the m = 2 spectrum appears to mimic the m = 1. The m = 0 shows a negative feature coinciding with the main m = 1 peak, the m = 0 spectrum is by definition, symmetric in n.

It would be a mistake to interpret all these features as representing independent modes existing in the plasma. Almost certainly virtually all the m = 2 spectrum should be regarded as arising from the toroidal linear

coupling effects previously discussed. The m = 0 feature must also be regarded as spurious for two reasons: first, it is negative, whereas in the idealised case the spectrum would be positive definite; second, there can be no $\tilde{B}_\theta$ component of a true m = 0, n ≠ 0 perturbation outside the plasma since there curl $\vec{\tilde{B}}$ = 0. Thus the m = 0 spectrum here contains little power which we can interpret as 'true'.

The features on m = 1 near n = 0 and n ≃ +9 are less certain. Inspection of the correlation matrix reveals little evidence of opposite helicity modes so probably we should regard the n ≃ +9 feature as an artifact arising from linear coupling although we cannot rule out the possibility of its representing an independent mode. The m = 1 n ~ 0 may well be a true mode, in which case it represents an equilibrium shift type of behaviour. However it may partly arise from the sidelobes of the convolution function.

Fig 15 shows the association spectrum for $\tilde{B}_\phi$ obtained from the internal poloidal array and the toroidal array. The m = 1 component looks similar to the $\tilde{B}_\theta$ spectrum although the peak is now near n = -10. This, we believe, should be interpreted as a bias effect in that $\tilde{B}_\phi$ is more sensitive to high $|n|$ and $\tilde{B}_\theta$ to low $|n|$ because of the direction of the perturbed field for a given mode at the edge (which is given by curl $\vec{\tilde{B}}$ = 0). The m = 2 spectrum is much smaller than for $\tilde{B}_\theta$, consistent with a weaker toroidal distortion. There is still a negative feature on m = 0 slightly shifted with respect to

the n = -10 peak; we regard this phase shift as an effect due to incomplete cancellation of liner induced phase shifts. The m = 1 n = +10 peak is much less significant than with $\tilde{B}_\theta$ consistent with its interpretation as a toroidal distortion artifact. There then remains the m = 0 n ~ 0 component which we take as real and indicating a definite contribution from those modes; and m = 1 n ~ 0 which is probably mostly toroidal distortion of the m = 0 n ~ 0.

It should be noted that these association spectra are corrected for liner penetration effects only by assuming a single 10 μs penetration time for the liner, whereas the theoretical liner penetration time (see Appendix) is different for different modes. In particular for m = 0 n = 0 the penetration time is about ten times longer for $\tilde{B}_\phi$, causing attenuation by a factor of ten. If this effect is allowed for, the m = 0 n ~ 0 feature on B_ϕ is significantly enhanced over that shown.

3.5 Evolutionary Phenomena

Several important phenomena have not so far been mentioned in our presentation of the results. First it must be noted that our statistical techniques have concentrated on frequencies above about 5 kHz which are high enough to exclude the global evolution of the equilibrium plasma parameters such as current and flux etc. However it is observed that on a good proportion of discharges there exist evolutionary phenomena at frequencies as low as 1 kHz which justify the designation 'perturbation' since they are not simply evolutions of a quasi-cylindrical equilibrium.

Because these turn out to be spatially fairly coherent, even though they exist for typically no more than one time cycle, we can illustrate their characteristics by plotting directly the temporal evolution of the edge field profiles. Fig 16 shows a particularly clear example of polar plots from a single discharge of the toroidal field amplitude as a function of θ referred to the mean B_ϕ at each θ (over the time plotted) as zero. The clear m = 1 character slowly rotating in azimuth is evident by inspection. Such perturbations as this are also evident on the toroidal array and indicate that it is again a helical perturbation with typical toroidal wavenumber $n \sim -10$. The (peak) amplitude of the mode is sometimes as great as $\tilde{B}_\phi/|B| \sim 5\%$ which for typical reversal levels is $\tilde{B}_\phi/|B_\phi|_a \sim 50\%$. These perturbations tend to be present only during the first msec or so of the sustainment phase, their amplitude decaying with time.

A second characteristic which must be emphasised under the heading of evolutionary phenomena concerns the various spectra presented earlier. These are time and shot averages over typically 1 ms and 5 - 10 shots. However we find that the characteristics of the fluctuations vary with time in a systematic though not reproducible manner. The fluctuations occur in bursts separated by quieter periods and are not in the statistical sense stationary random signals. One striking observation is a form of cyclic behaviour in the evolution of the n-spectrum. Fig 17 shows the evolution of the n-spectrum calculated by a sliding average over 128 μs during a period of 0.6 ms in the sustainment phase. During this period the spectrum evolves from single-peaked high power to double-peaked lower power and back again, going through about two cycles in 0.6 ms. The average spectra of Fig 11 are dominated at lower frequencies by the higher power single peaked type of spectrum but it it evident that at some times other wave numbers are dominant.

Finally, we should make some observations concerning the termination phase. As Fig 2 illustrates, the amplitude of fluctuations rises considerably once reversal is lost. In Fig 18 we show on a relative scale how the fluctuation power spectrum during termination differs from that during sustainment. The shape is significantly altered, showing a rise up to ~ 50 kHz; thus higher frequencies become more important. Another characteristic of the termination phase is that the rotation is much more coherent. This shows clearly on the time delayed cross correlations illustrated in Fig 19. The rotations are always in the same direction during termination viz toroidally in the direction of electron current flow, poloidally in the electron diamagnetic drift direction (these directions are equivalent for our helical perturbations).

Another effect which shows clearly in Fig 19 is that the toroidal wavelength (and coherence length) increase. This is a progressive effect but of course our figure only captures one period during the current decay. At the time of Fig 19 the Θ is about 1.0. The poloidal structure is always dominantly m = 1 and the helicity corresponds to negative n; for Fig 19 n ~ -3 to 4 for B_ϕ and ~ -1 to 2 for B_θ.

4. DISCUSSION

Our measurements show that the overwhelming proportion of the fluctuations observed at the plasma edge are attributable to low poloidal mode numbers M_0 and M_1. Of course, the nature of the measurements tends to

favour large scale perturbations such as these, since fine scale perturbations originating well inside the plasma will generally fall off more rapidly with radius and would therefore be proportionately smaller at the edge. Nevertheless, the fact that the fluctuation power in Fourier modes $m > 2$ is only about 3% of that in modes $m \lesssim 2$ for B_ϕ appears to be a quite strong indication that the low m modes are indeed dominant throughout the plasma.

The difference for $m > 0$ between the poloidal mode spectra for $\tilde{B}_\theta$ and $\tilde{B}_\phi$ is explicable by consideration of the details of the toroidal distortion effects. Writing the condition curl $\vec{\tilde{B}} = 0$ in toroidal geometry provides a relationship between the fields outside the plasma for a given helical mode; so that for example if $\tilde{B}_\phi$ is purely $m = 1$ then $\tilde{B}_\theta$ has an $m = 2$ component of amplitude a/R. The outward (Shafranov) shift of the plasma in the shell is at least partly responsible for these toroidal distortions but this cannot easily be distinguished from departure of the internal mode structure from the quasi cylindrical approximation.

A major advance in the present results is the detailed information we have obtained on the toroidal mode structure. In order to see its significance we must consider the radial profile of the field line pitch which we express in terms of the safety factor $q \equiv rB_\phi/RB_\theta$. As is well known the RFP adopts a field configuration in which the profile may be estimated by using one of the quasi-cylindrical models such as the modified Bessel Function Model or the Bessel Vacuum model. For the HBTX1A discharges of interest here such calculations indicate the on-axis q_0 to be about 1/5 and q falls to zero at $r/a \sim 0.75$, the reversal point; at the liner it

reaches $q \simeq -0.04$. Internal magnetic probe measurements on different discharges confirm these estimates which are relatively insensitive to the model employed.

Now helical perturbations are resonant at the radius where $q = -m/n$ which for $m = 1$ is where $q^{-1} = -n$. At this radius, non-zero radial field perturbations will lead to magnetic island formation. Our main peak in the n spectrum at $n \sim -10$ is a mode which is resonant at $r/a \sim 0.5$ and the broad spectrum we see which extends from $n \sim 5$ to $n \sim -20$ indicates modes which are resonant at radii from $r \sim 0$ out to quite close to the reversal surface. We cannot, with our modest resolution, exclude modes which are non-resonant (i.e. $\left|\frac{n}{m}\right| < 5$) but their contribution, if any, is small. In addition to these $m = 1$ modes the $m = 0$ perturbations are always resonant at the reversal surface.

The perturbations we see seem to correspond qualitatively quite well with the expectations of resistive instability theory [9] in that we see $m \doteq 1$ perturbations resonant from $r = 0$ outward and also $m = 0$ perturbations of long toroidal wavelength. For the discharges studied here we have not observed perturbations resonant outside the reversal surface ($m = 1$ $n \gtrsim +25$) although the statistical accuracy of our measurements only allows us to put an upper bound of 5% of the fluctuation power in such modes. This corresponds to an r.m.s. amplitude upper bound of $\tilde{B}/|B| < 0.2\%$.

Our present analysis does not allow us to distinguish whether the $m = 0$ perturbations arise directly from linearly unstable resistive modes or indirectly as a non linear consequence of the $m = 1$ modes. Further studies employing higher order correlations and focusing on the time non-

stationarity may be able to shed further light on this topic. Nor are we able to distinguish the driving energy sources for any of the perturbations which provide the usual theoretical distinction between tearing and pressure driven 'g' modes.

One may obtain an estimate of the growth (and decay) times for these perturbations from the frequency spectra presented. If we take the width of the overall spectrum as the relevant frequency spread i.e. ~ 30 kHz one would estimate a growth time of ~ 5 μs. This might be rather shorter than the required estimate since the relevant frequency width might more appropriately be taken as the width of the individual features on the spectrum i.e. more like 5 kHz leading to ~ 30 μs. This should be compared with the poloidal Alfvèn transit time of ~ 0.5 μs for these discharges and magnetic Reynolds number $S \sim 10^5$. Thus the perturbation lifetime is approximately $S^{-1/3}$ (in resistive time units) although this is only a single measurement, not a scaling. This lifetime suggests that we should take the perturbations as dominantly 'resistive' rather than 'ideal' MHD in character. Of course, the states we are observing are non linear so that this distinction is of debatable significance except that we may assume that magnetic reconnection and island formation are occurring. This resistive character has been qualitatively confirmed by observations of radial magnetic field perturbations inside the plasma on HBTX1A as well as elsewhere [6]; i.e. $\tilde{B}_r$ does not reverse sign inside the plasma.

In order to estimate the size of magnetic islands inside the plasma arising from a specific helicity mode we could in principle integrate the linearized MHD equations inward from the edge till we reach the resonant

surface. The island width, W, may then be estimated from the standard formula [11]

$$W = 4\left| \frac{\tilde{B}_r r_s}{m B_\theta} \quad \frac{q}{q'} \right|^{\frac{1}{2}}$$

This would require detailed knowledge (or assumption) of the equilibrium field profiles in order to carry out the integration. We may instead get an order of magnitude estimate by appealing to the observation that theoretical studies [9] of tearing mode stability perform essentially this integration and indicate that, roughly speaking, the radial derivative of $\tilde{B}_r$ is approximately constant outside the resonant surface, for modes whose resonant surface is not too close to the axis. Now we measure the perturbations close to the shell where $\tilde{B}_r = 0$ so $\underline{\nabla}.\underline{B} = 0$ gives

$$\left|\frac{\partial \tilde{B}_r}{\partial r}\right| = \left| \frac{m}{r}\tilde{B}_\theta + \frac{n}{R}\tilde{B}_\phi \right|$$

thus our estimate is

$$\tilde{B}_r(r_s) = (a - r_s)\left| \frac{m}{r}\tilde{B}_\theta + \frac{n}{R}\tilde{B}_\phi \right|_a$$

For $n \sim -10$ $(m = 1)$, typically $\left|q/q' r_s\right| \simeq 1$ and $B_\theta(r_s) \sim 1.5\left|B(a)\right|$ so

$$W/r_s \simeq 4\left\{ (a - r_s)\left| \frac{m}{r}\tilde{B}_\theta + \frac{n}{R}\tilde{B}_\phi \right|_a / m B_\theta(r_s) \right\}^{\frac{1}{2}} \sim 4\left|\tilde{B}/B\right|_a^{\frac{1}{2}}$$

In order to determine the amplitude $\left|\tilde{B}\right|$ to be ascribed to each mode take ½

of the ~ 2% rms fluctuation level as being in m = 1 and take this as spread over about 6 toroidal modes as indicated by the n spectrum this then indicates a single mode r.m.s. level of $2/\sqrt{12} \simeq 0.5\%$. Hence the above estimate of island size is $W/r_s \sim 0.3$.

The separation, δ, of (m = 1) resonant surfaces in this region of the plasma is given by

$$\delta = q^2/q' \sim r_s \sim 0.1\ r_s$$

Therefore the island overlap condition [13] $W > \delta$ is easily satisfied so if the different helicities are simultaneously present with this typical amplitude we expect that the magnetic field lines are stochastic throughout the region and magnetic surfaces no longer exist. Strictly, our analysis has not shown unequivocally that the different helicities are truly simultaneous in view of the 'bursting' character of the fluctuations; however it seems most improbable that the different modes would be sufficiently separated in time for stochasticity to be avoided. Estimates of m = 0 island sizes give similar values for W, though in this case we are less certain of the resistive MHD mode character. Much of the M_0 mode power may arise non-linearly from the M_1.

Given the mode amplitudes and the fact that field lines are stochastic we can estimate the energy transport due to stochastic diffusion. The field line diffusion coefficient [12] is, for our case, typically $\langle \Delta r^2/L \rangle \sim a\left|\tilde{B}/B\right|_a^2$ giving effective perpendicular energy diffusivity [13] $\chi_{eff} \sim v_e \langle \Delta r^2/L \rangle$ where v_e is the electron thermal speed. For $\left|\tilde{B}/B\right|_a = 0.01$ and

$T_e \sim 100$ eV this leads to an estimate of energy confinement time $\tau_E \sim 50$ μs assuming the whole of the plasma experiences this stochastic diffusion. This value is consistent with experimentally observed parameters. However it should be regarded as an order of magnitude estimate only because of the sensitive (squared) dependence on the internal $\tilde{B}_r$ which has been estimated somewhat crudely. Nevertheless it should be emphasised that this is a direct estimate based on measured longitudinal correlation lengths and field perturbation amplitudes and not, like earlier stochastic transport estimates [5, 14], on theoretical estimates of longitudinal correlation.

It is of interest too to estimate the island size for the large coherent slowly rotating perturbations of Fig 16. The linearized estimates are somewhat questionable for such large perturbations but taking the peak perturbation amplitude we obtain $W \sim r_s$, indicating a very large island but not extending to the magnetic axis. More careful non-linear calculations might be appropriate in this case to obtain more reliable estimates.

The rotation speeds observed are of the same order of magnitude as estimates of diamagnetic drifts. However the ambiguity of direction observed indicates that a simple interpretation in terms of these drifts is hardly adequate. It should be noted also that an electrostatic potential of about 100 V would be sufficient to cause plasma rotation of this order of magnitude.

The rather cyclic behaviour observed in the evolution of the n-spectrum leads one to a rather persuasive picture of the overall behaviour. Suppose that the evolution of the field profiles leads to a situation in which

resistive modes at r/a ~ 0.5 are preferentially destabilised. These grow and then stabilise themselves via non linear modifications to the profiles; their amplitude then decreases. However the profile modifications tend to destabilise other modes with n greater (and smaller) than those just discussed. Therefore these other modes tend to become dominant and enforce profile changes which compete with those of the first modes. This competition continues, establishing a quasi-equilibrium in which cyclic variations of mode amplitude maintain the mean profile such that no mode achieves complete dominance. Theoretical ideas of this sort have been proposed [15] in the context of the Tokamak disruptive instability. However, here we seem to have direct experimental evidence in the RFP for the importance of this MHD mode competition.

Many further fluctuation topics remain to be investigated; notably, how the amplitudes and character of the perturbations vary with plasma parameters and also what are the non-linear characteristics, mode coupling and so forth. However, the present study has revealed many interesting and significant characteristics of the magnetic fluctuation structure in the RFP, which should serve as a basis from which to pursue these investigations.

ACKNOWLEDGEMENTS

We are grateful to the other members of the HBTX1A team for their co-operation and to J B Taylor for helpful discussions.

REFERENCES

[1] Rusbridge M G, Lees D J and Saunders P A H: Nucl Fusion Suppl. pt 3, 895 (1962).

[2] Rusbridge M G, Jones H W, Lees D J, Saunders P A H and Witalis E A: Plasma Phys. 3, 98 (1961).

[3] Robinson D C and Rusbridge M G: Phys. Fluids 14, 2499 (1971).

[4] Carolan P G, Gowers C W, Robinson D C, Watts M R C and Bodin H A B: in "Plasma Physics and Controlled Nuclear Fusion Research" (Proc 7th Int. Conf. Innsbruck, 1978) Vol 2, IAEA Vienna (1979) 23.

[5] Antoni V and Ortolani S: to be published in Plasma Physics.

[6] Tamano T, Carlstrom T, Chu C, Goforth R, Jackson G, LaHaye R, Ohkawa T, Schaffer M, Taylor P, Brooks N and Chase R: in "Plasma Physics and Controlled Nuclear Fusion Research" (Proc 9th Int Conf Baltimore 1982) Vol 1, IAEA Vienna (1983) 609.

[7] eg Hutchinson I H: Phys Rev Lett 37, 338 (1976)

[8] Robinson D C: Nucl Fusion 18, 939 (1978).

[9] Robinson D C: Plasma Phys. 13, 439 (1971).

[10] Bodin H A B, Bunting C A, Carolan P G, Giudicotti L, Gowers C W, Hirano Y, Hutchinson I H, Jones P A, Lamb C, Malacarne M, Newton A A, Piotrowicz V A, Shimada T and Watts M R C: in "Plasma Physics and Controlled Nuclear Fusion Research" (Proc 9th Int Conf Baltimore 1982) Vol 1 IAEA Vienna (1983) p641.

[11] eg Bateman G: "MHD Instabilities" MIT press, Cambridge Ma. (1978).

[12] Rosenbluth M N, Sagdeev R Z, Taylor J B and Zaslavski G M: Nucl Fusion 6, 297 (1966).

[13] Rochester A B and Rosenbluth M N: Phys Rev Lett 40, 38 (1978).

[14] Hender T C and Robinson D C: Computer Phys Comm 24, 413 (1981).

[15] Furth H P: in "Current Disruption in Toroidal Devices" Lackner K and Zehrfeld H P (Eds) IPP 3/51. Max Planck Institut für Plasmaphysik, Garching (1979).

APPENDIX

Because some of our measurements are made outside the liner it is important to estimate the effect of the liner on the observed fluctuations. If we treat the liner as thin with conductivity σ and thickness δ having radius a concentric within a shell, assumed infinitely conducting, of radius b and consider perturbations of the form exp $i(m\theta + n\phi - \omega t)$. Then provided

$$\left[\left(\frac{m}{a}\right)^2 + \left(\frac{n}{R}\right)^2\right](b - a)^2 \ll 1$$

we can treat the outward penetration of magnetic field across the liner (B_o) as related to that inside (B_i) by:

$$B_o = B_i/(1 + i\omega\tau)$$

where

$$\tau = \mu_o \sigma \delta (b - a)$$

This shows that the effect of the liner is to integrate the field with a passive time constant τ.

An important complication is that the liner has bellows construction so that the effective δ is different for currents flowing in the poloidal and toroidal directions. Denote these by δ_θ, δ_ϕ then it may be shown that, approximating the liner as thin, we have

$$\delta_{eff} = \frac{\delta_\theta \delta_\phi \left[(m/a)^2 + (n/R)^2\right]}{\delta_\theta (m/a)^2 + \delta_\phi (n/R)^2}$$

For the liner of HBTX1A $\tau_\theta = \mu_o \sigma \delta_\theta (b - a) \simeq 30$ μs and $\delta_\phi \simeq \delta_\theta/16$ from which the penetration time constant of any mode may be calculated. For example if $m = 0$ $n \neq 0$ $\tau = 30$ μs while for $m = 1$, $n = 8$ $\tau \simeq 10$μs, corresponding to frequencies ~ 5 kHz and 15 kHz respectively.

Additional complications arise because the convolution depth is not small compared to (b - a); however the above treatment is regarded as sufficient to first order. Finally, for $m = 0$ $n = 0$ the shell's gaps prevent it from acting as a flux conserver and the penetration time depends on the equivalent flux out to the windings. The penetration times are then estimated as ~ 100 μs for B_z and ~ 20 μs for B_θ. It should be noted therefore, that $m = 0$ perturbations (and particularly for $n = 0$) suffer significantly greater attenuation in general than those for higher m.

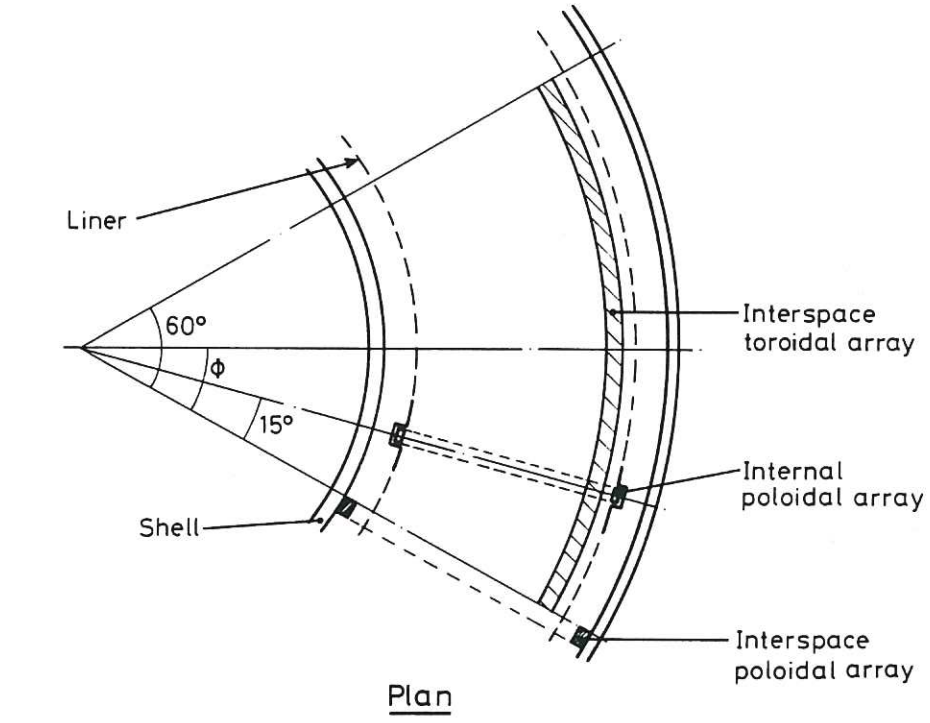

Plan

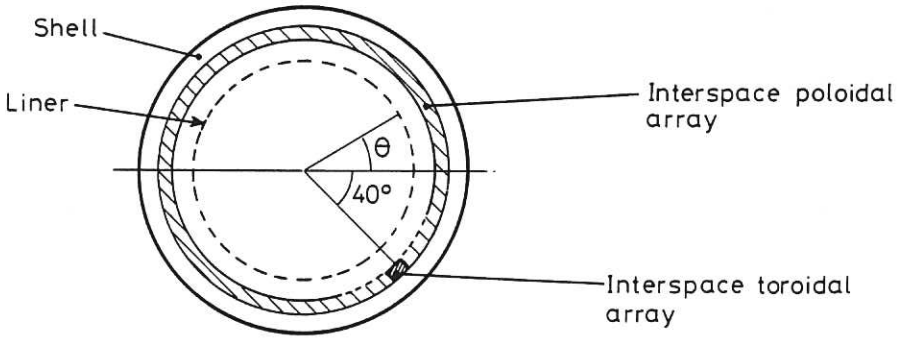

Section

Fig.1 Discrete coil layout.

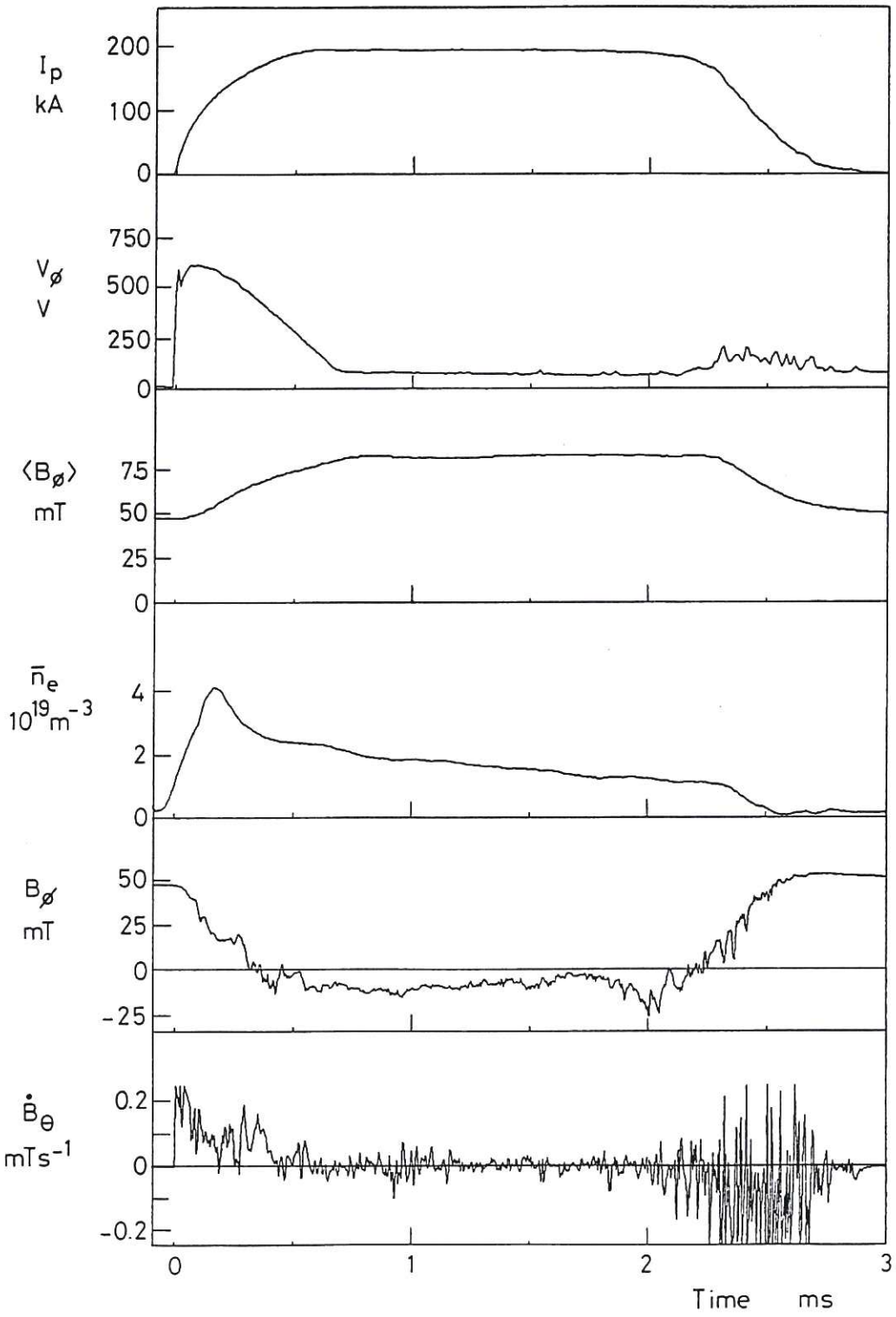

Fig.2 Time history of a typical shot: plasma current (I_p); toroidal loop voltage (V_ϕ); average toroidal magnetic field ($<B_\phi>$); average line-of-sight electron density ($\bar{n}_e$); toroidal magnetic field at the liner (B_ϕ); time derivative of poloidal magnetic field at the liner ($\dot{B}_\theta$).

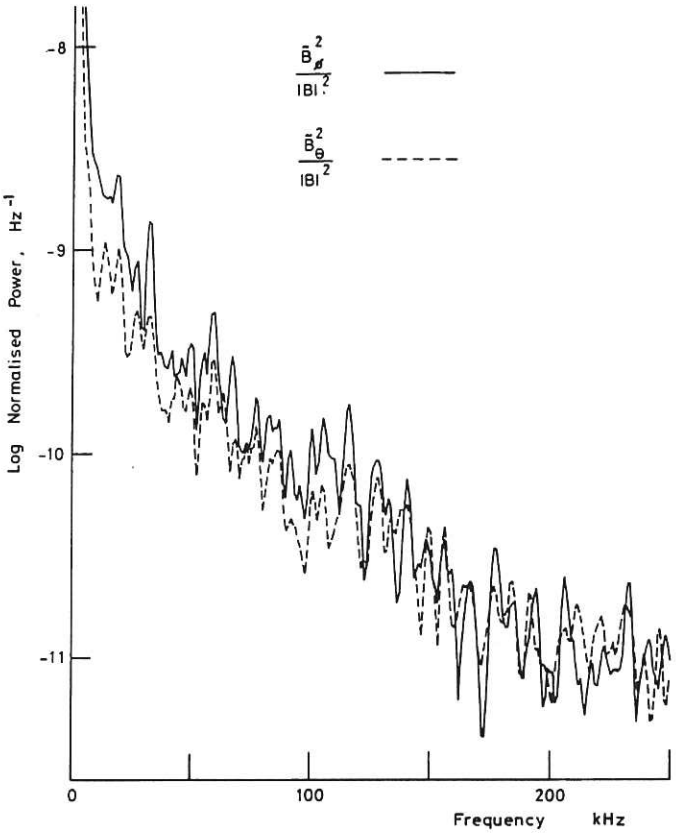

Fig.3 Power spectrum of $\widetilde{B}_\phi/|B|^2$ and $\widetilde{B}_\theta/|B|^2$ during the sustainment phase obtained from the internal coils ensemble averaged over 5 shots.

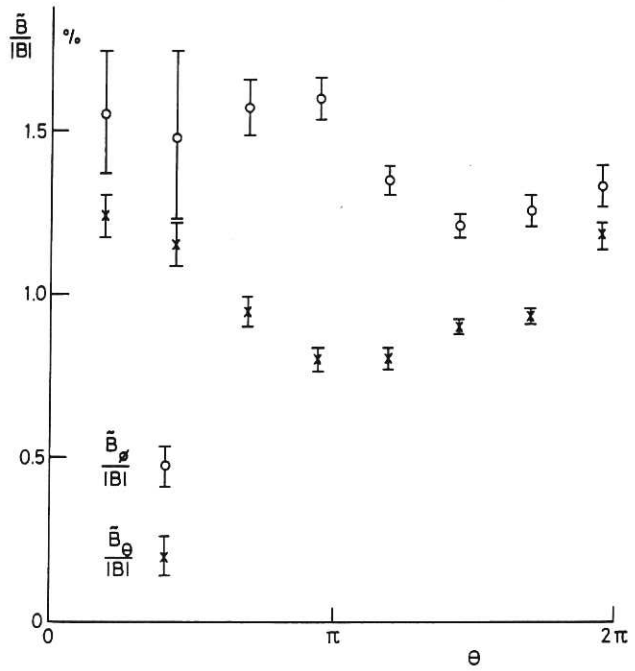

Fig.4 Ensemble averaged amplitude of $\widetilde{B}_\phi/|B|$ and $\widetilde{B}_\theta/|B|$ as a function of the poloidal angle during the sustainment phase, in frequency band 5–250 kHz.

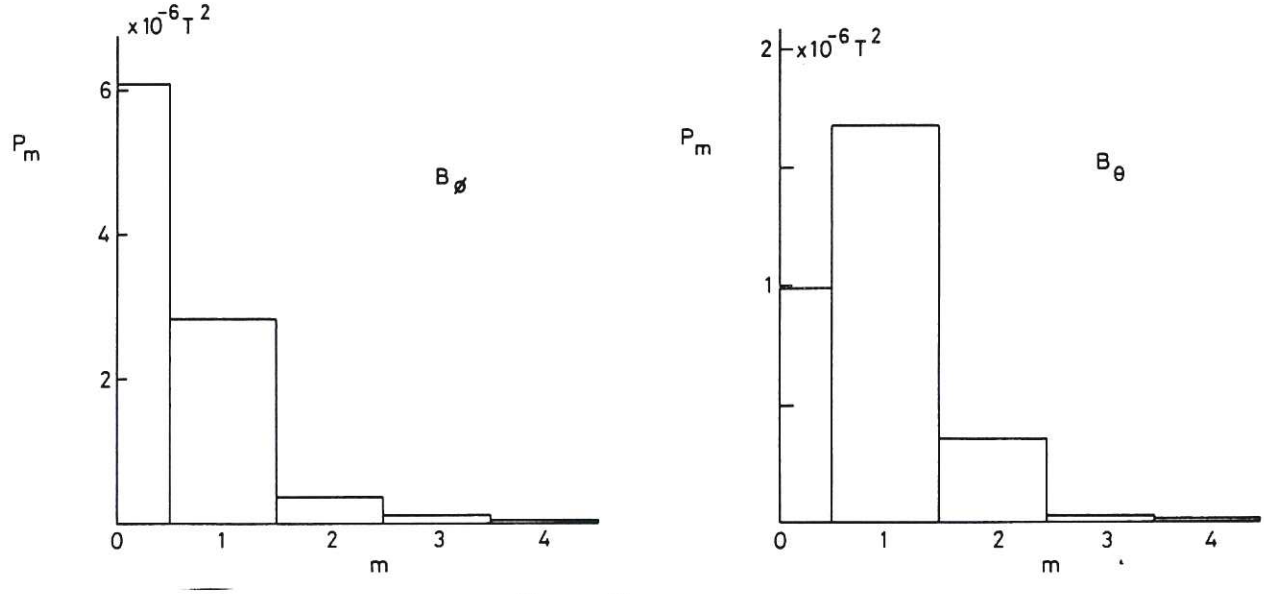

Fig.5 Poloidal mode power spectrum for $\widetilde{B}_\phi$ and $\widetilde{B}_\theta$ during the sustainment phase in the frequency band 5–250 kHz.

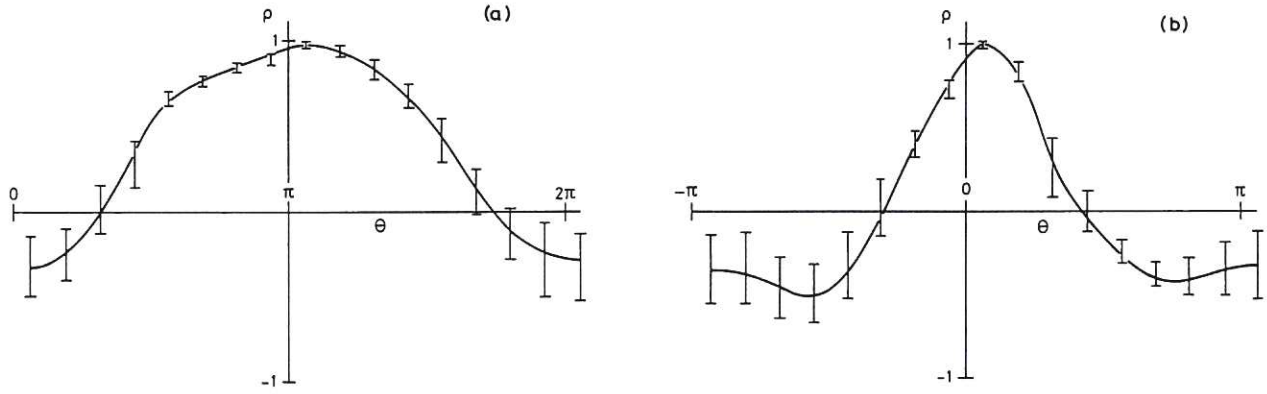

Fig.6 Equal time cross-correlation coefficient (spatial autocorrelation) for B_θ as a function of displacement in poloidal angle; (a) reference coil at $\theta \simeq \pi$; (b) reference coil at $\theta \simeq 0$. Sustainment phase: filter 5–50 kHz.

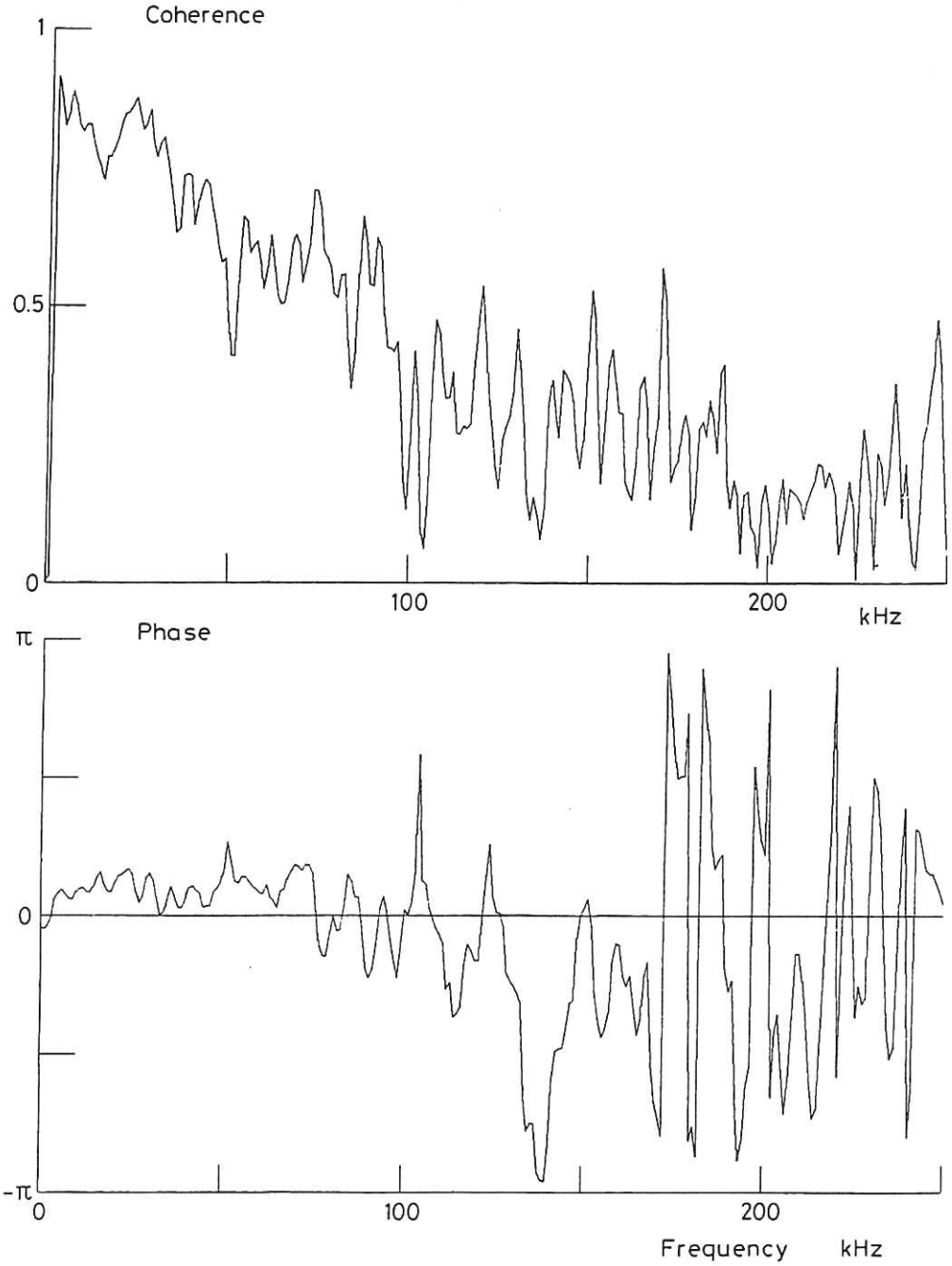

Fig.7 Coherence and cross-phase spectrum between the m = 1 and the m = 2 cosine modes for B_θ (ensemble average over 10 shots sliding averaged over 3 frequency points during sustainment phase).

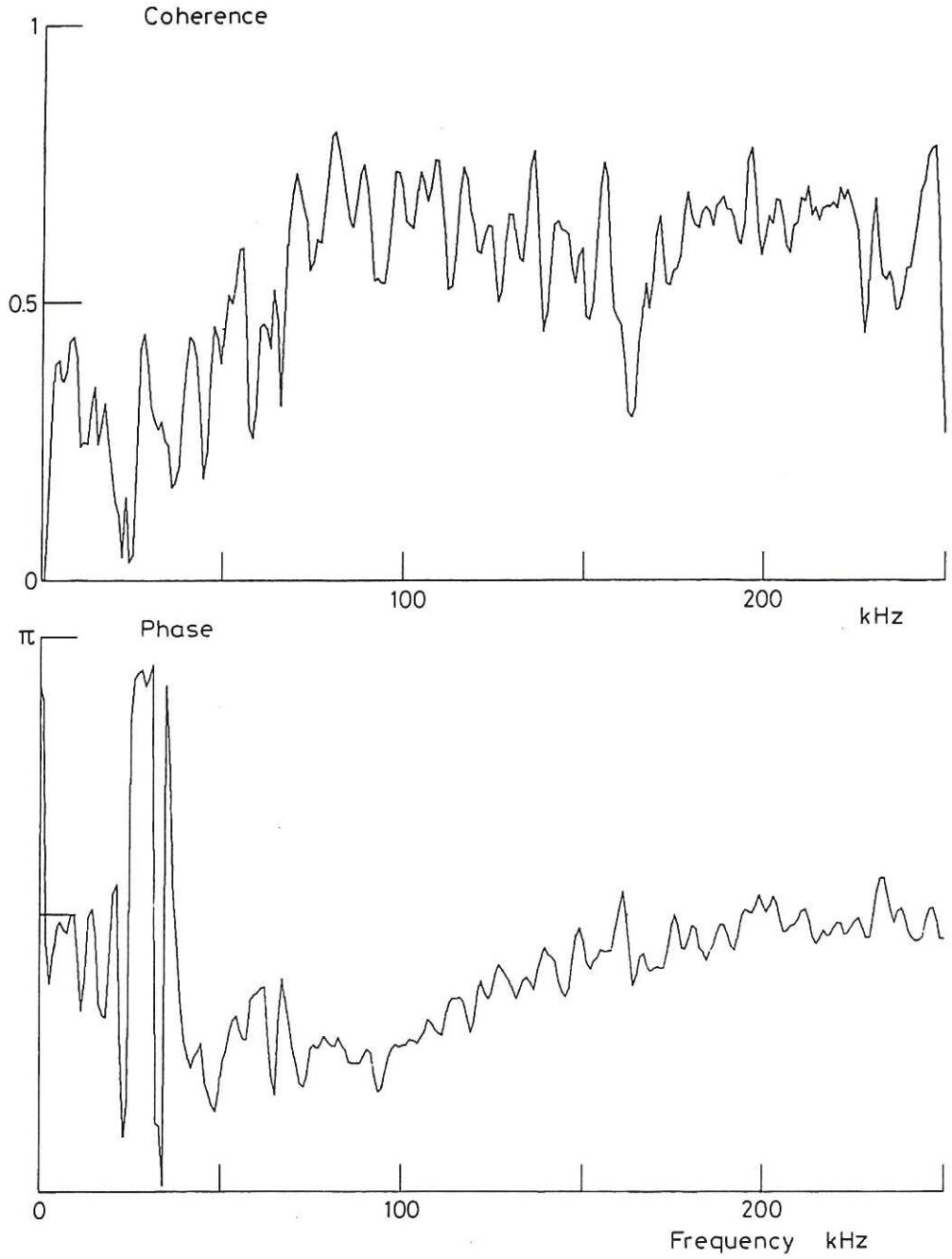

Fig.8 Coherence and cross-phase spectrum between the m = 0 and m = 1 cosine modes for $\widetilde{B}_\phi$ (averaged as in Fig.7).

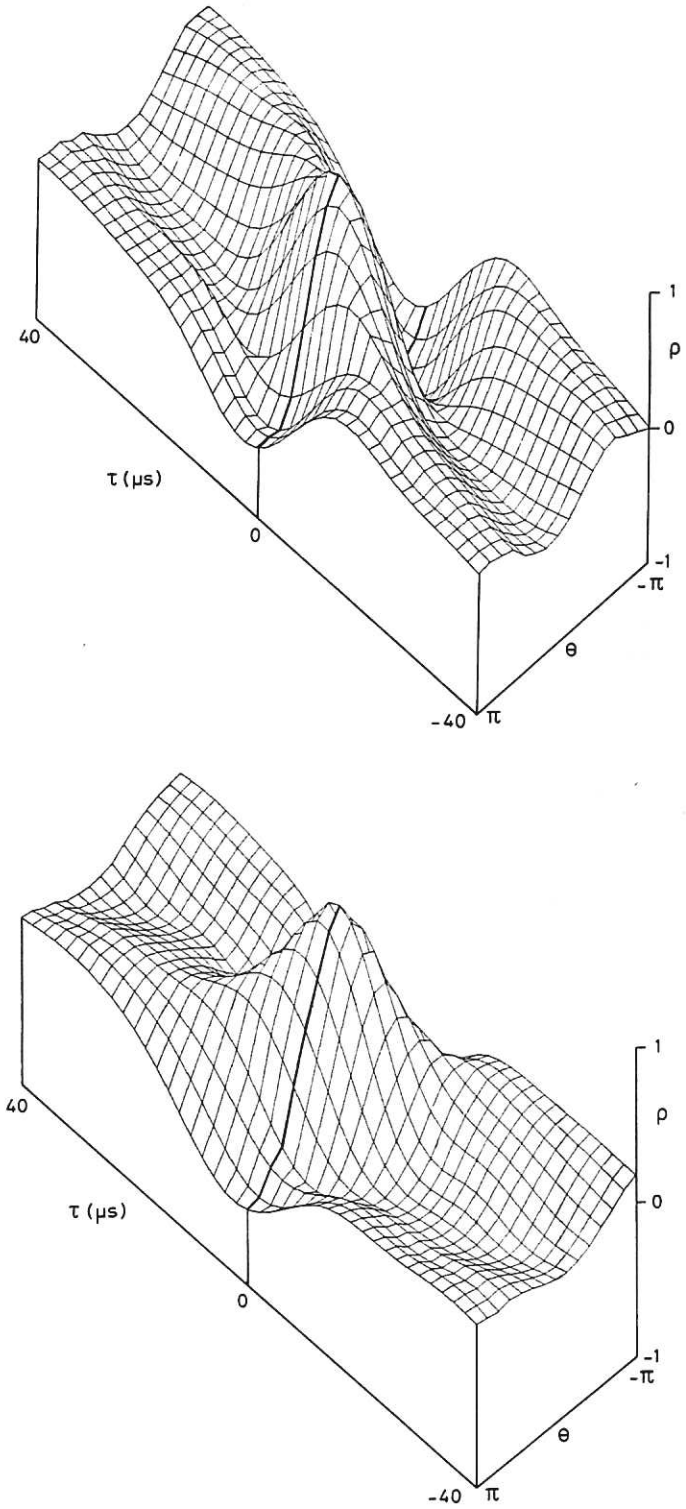

Fig.9 Time delayed cross-correlation coefficient as a function of θ, ensemble averaged over the sustainment phase, filter 5 – 50 kHz: (a) for $\widetilde{B}_\theta$ (b) for $\widetilde{B}_\phi$; showing evidence of poloidal rotation.

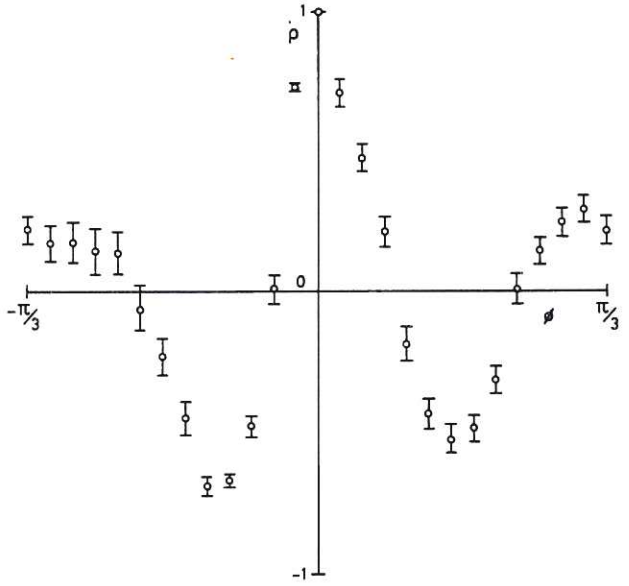

Fig.10 Autocorrelation in space, $\rho(\phi)$ for $\widetilde{B}_\phi$ (frequency band: 5 – 15 kHz).

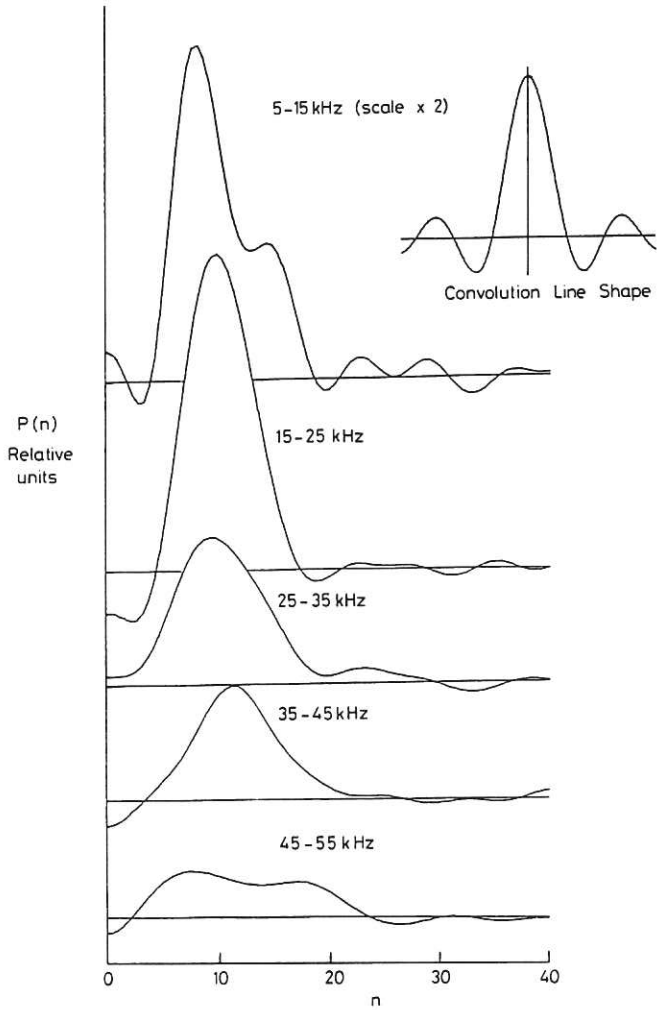

Fig.11 Toroidal mode power spectrum, for various frequency bands, of $\widetilde{B}_\phi$.

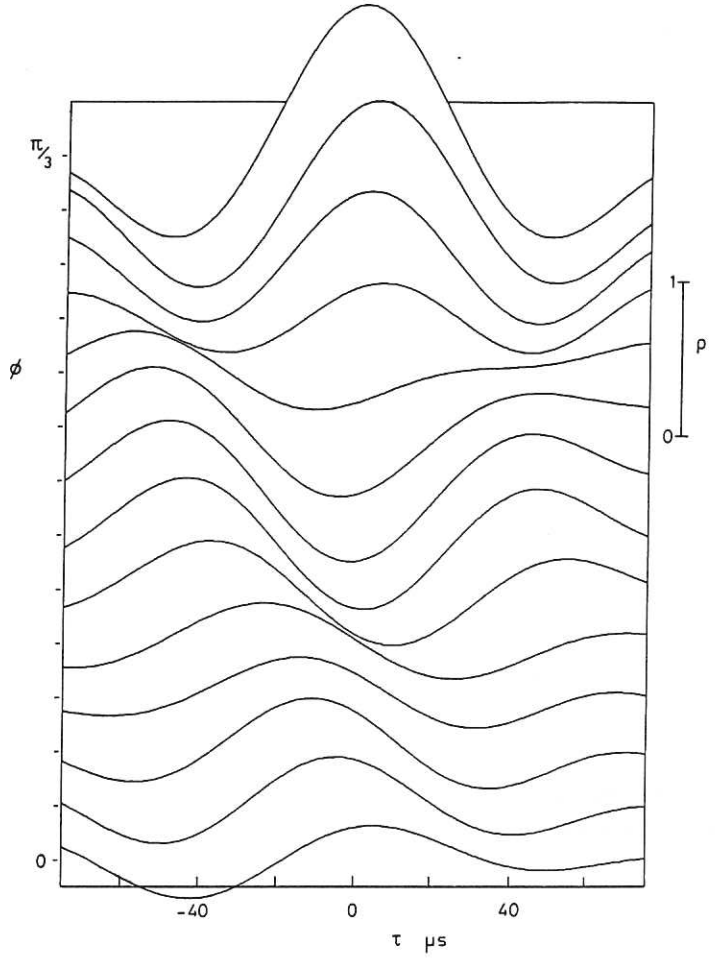

Fig.12 Correlation function ρ vs time delay, τ and toroidal angle, ϕ for $\tilde{B}_\phi$ (frequency band 5 – 15 kHz) showing evidence of toroidal rotation.

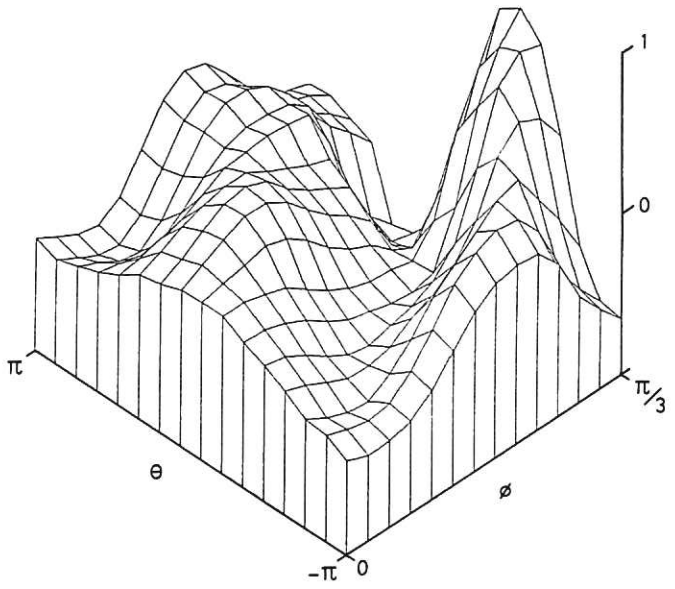

Fig.13 Correlation matrix between the poloidal and toroidal arrays for $\tilde{B}_\theta$ (frequency band 5 – 50 kHz, indicating dominantly helical structure.

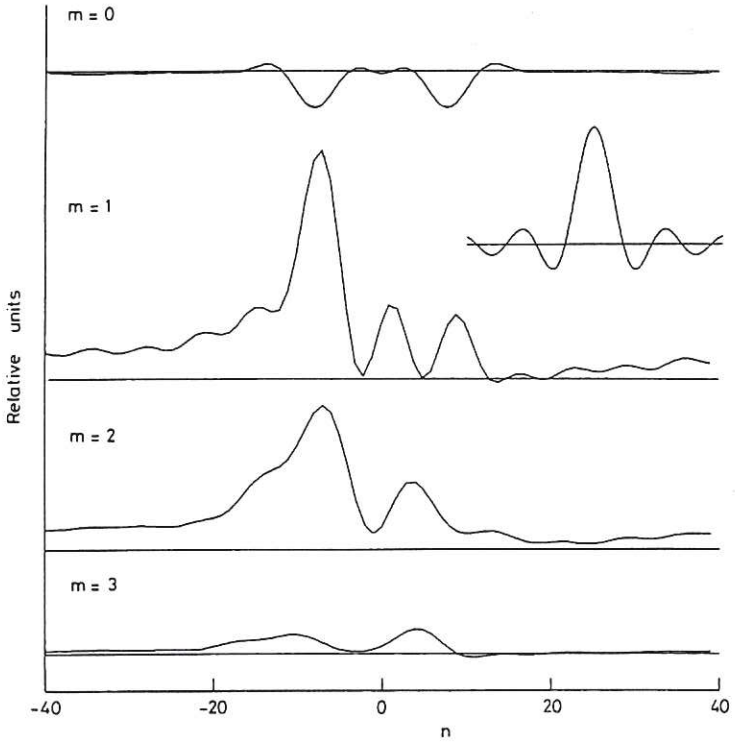

Fig.14 Association spectrum for $\widetilde{B}_\theta$. Inset shows convolution line function (frequency band 5 – 50 kHz).

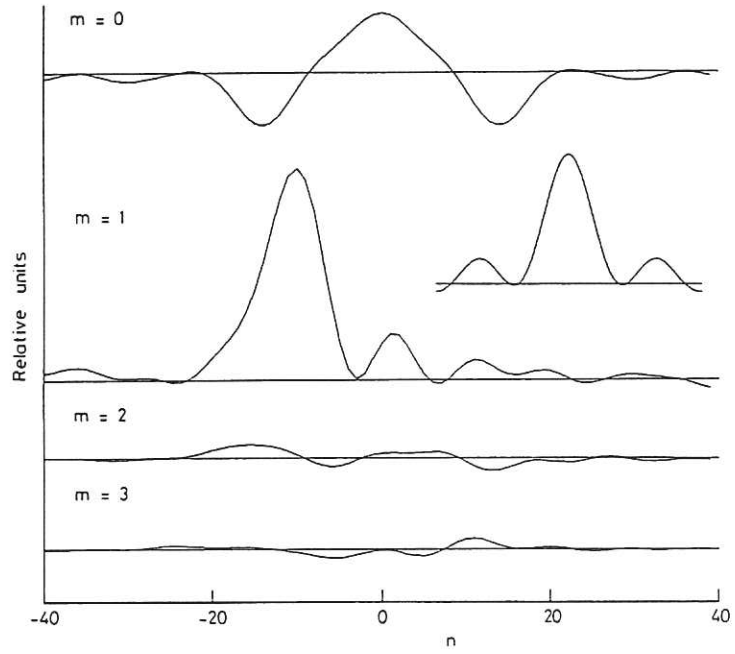

Fig.15 Association spectrum for $\widetilde{B}_\phi$. Inset shows convolution line function (frequency band 5 – 50 kHz).

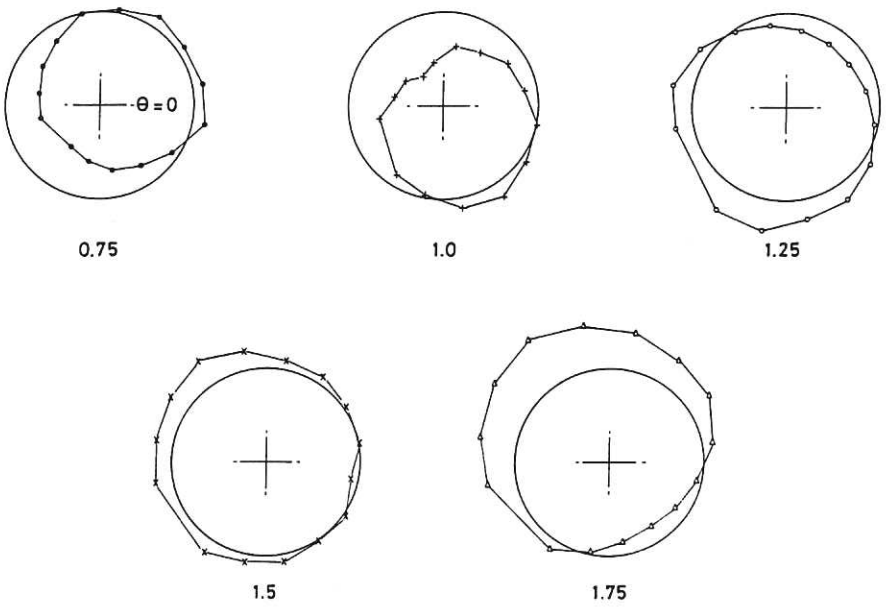

Fig.16 Polar plots of $\widetilde{B}_\phi$: evolution in time (ms) showing low frequency m = 1 rotation.

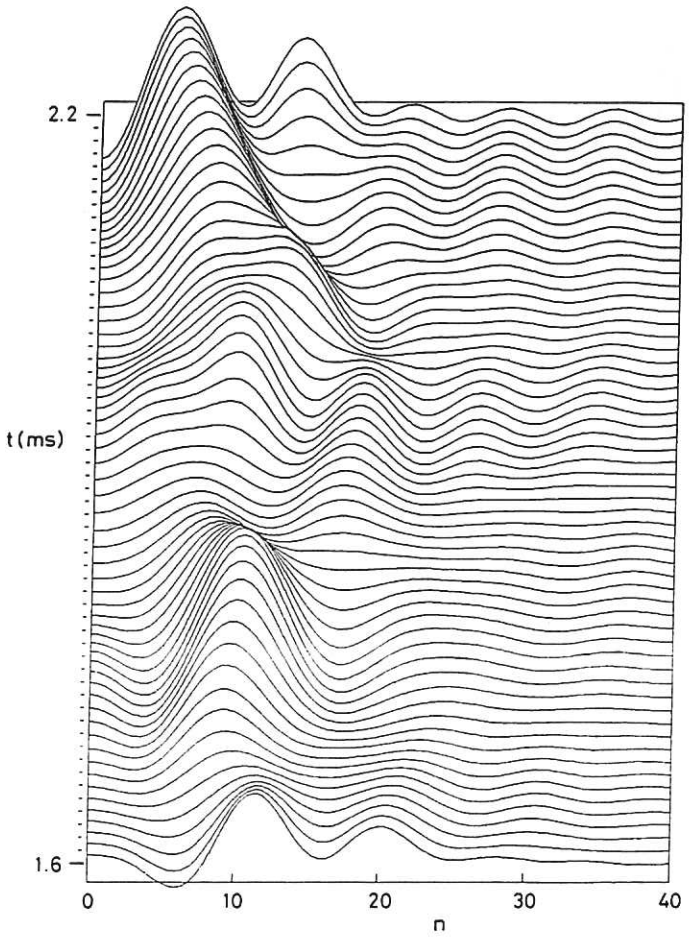

Fig.17 Time evolution of n-spectrum for $\widetilde{B}_\phi$ (frequency band 5 – 50 kHz).

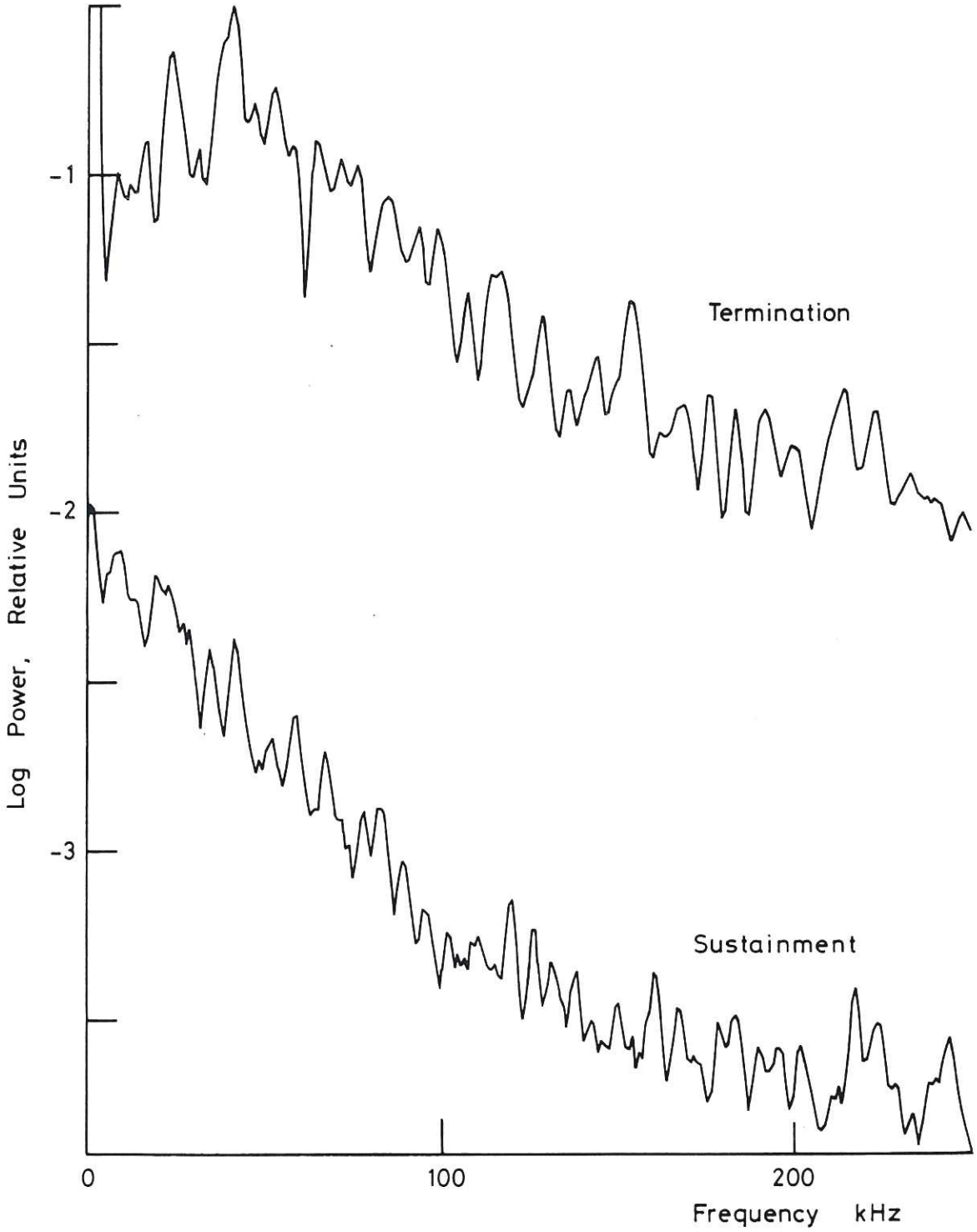

Fig.18 Relative power spectra for $\widetilde{B}_\theta$ during the sustainment phase and termination.

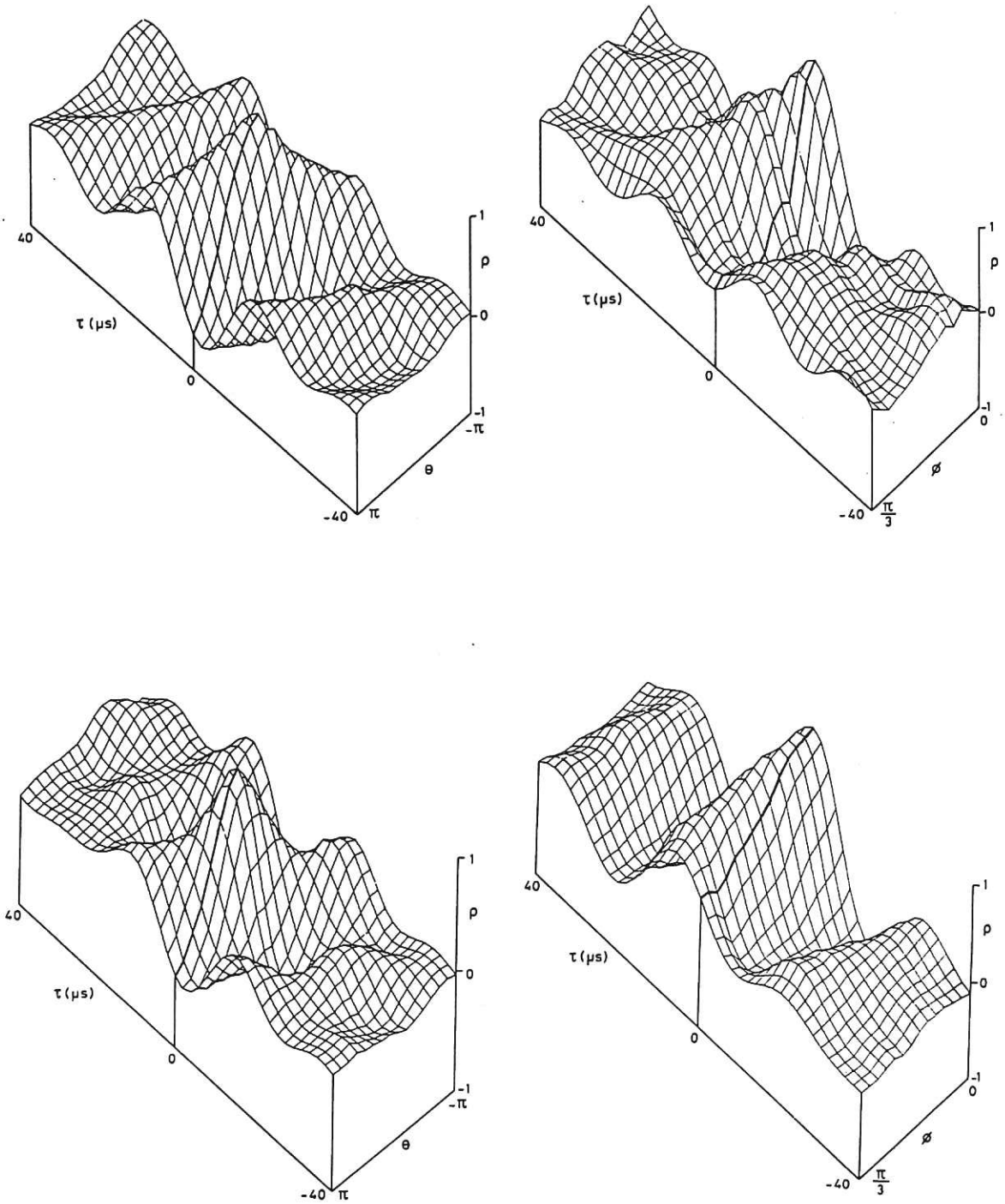

Fig.19 Time delayed cross-correlation coefficient for $\widetilde{B}_\phi$ (top) and $\widetilde{B}_\theta$ (bottom) as a function of θ (left) and ϕ (right) during the termination phase (filter 5 – 50 kHz).